Polymer Journal (2024) 56:205–214
https://doi.org/10.1038/s41428-023-00856-8

ORIGINAL ARTICLE

Effects of different types of functionalized polypropylenes on the tensile strength of short carbon fiber-reinforced polypropylene composites

Ayaka Yamaguchi[1,2] · Hideyuki Uematsu[3] · Toshikazu Sakaguchi[2] · Tamotsu Hashimoto[2]

Received: 5 September 2023 / Revised: 29 October 2023 / Accepted: 30 October 2023 / Published online: 21 December 2023

Abstract

In this study, the effects of various functionalized polypropylenes (PPs) with different types and contents of functional groups and crystallinities on the tensile strength of short carbon fiber (SCF)-reinforced plastics (SCFRPs) prepared by injection molding were evaluated. The tensile strengths of SCFRPs were significantly influenced by interfacial adhesion. The types and contents of functional groups introduced into functionalized PP were the dominant factors impacting the development of interfacial adhesion. In particular, near the surface where SCF and PP were highly oriented in parallel, functionalized PP with more functional groups added to side chains exhibited higher interfacial adhesion than that with fewer functional groups. These results suggested that PP molecular chain orientations resulting from the shear flow of injection molding were among the key factors affecting the interfacial adhesion of the PP matrix.

Introduction

Recently, carbon fiber (CF)-reinforced plastics have witnessed increasing demand and usage owing to their numerous advantages. The compositions of the reinforcements vary from continuous to short CFs (SCFs). SCF-reinforced plastics (SCFRPs) have been developed to fill the gaps in the mechanical properties of continuous-fiber laminates and unreinforced plastics [1]. SCFRPs offer several benefits because of their ease of fabrication, economy, and excellent mechanical properties. The fabrication process of SCFRP materials involves extrusion compounding and injection molding [1–4]. Among thermoplastic polymers, polypropylene (PP) is produced in large quantities due to its ease of processing, thermal stability, low density, and low cost. Correspondingly, the usage level of CF-reinforced PP composites is expected to increase.

Numerous studies have focused on the effects of the fiber content and/or length to enhance the mechanical properties of SCFRP composites [1–9]. Better mechanical properties, such as tensile strength and modulus, can be achieved by increasing the SCF content and length. However, the fiber length tends to decrease with increasing SCF content in SCFRPs owing to the fiber–fiber interactions, resulting in a low fiber reinforcing efficiency [3, 4]. In addition, the mechanical properties of short fiber-reinforced composites are affected by fiber orientation [9] and fiber dispersity [10, 11]. Therefore, the content, length, dispersity, and orientation of SCFs are critical factors determining the mechanical properties of SCFRPs.

The interfacial adhesion between fibers and the polymer matrix is a key parameter that determines the properties of fiber-reinforced composites. However, PP has low polarity, and a high fiber–matrix interfacial adhesion cannot be expected. Therefore, research has been conducted on improving the interfacial adhesion properties between PP

Supplementary information The online version contains supplementary material available at https://doi.org/10.1038/s41428-023-00856-8.

✉ Ayaka Yamaguchi
yama1132@u-fukui.ac.jp

✉ Tamotsu Hashimoto
t.hashimoto@matse.u-fukui.ac.jp

[1] Technical Division, School of Engineering, University of Fukui, Bunkyo, Fukui 910-8507, Japan

[2] Department of Materials Science and Engineering, Graduate School of Engineering, University of Fukui, Bunkyo, Fukui 910-8507, Japan

[3] Research Center for Fibers and Materials, University of Fukui, Bunkyo, Fukui 910-8507, Japan

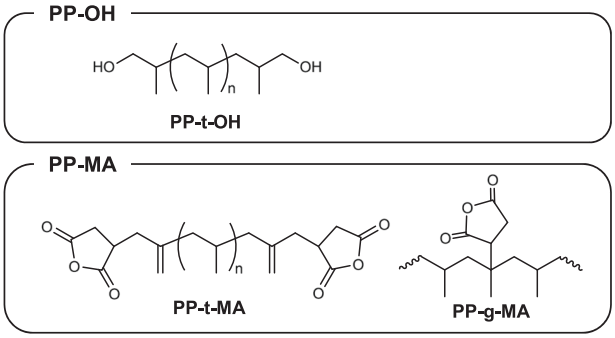

Scheme 1 Chemical structures of functionalized PPs

and CF via fiber surface modification [6, 12, 13] and the addition of functional compatibilizers into the PP matrix, with the most common variation being maleic anhydride-modified PP (PP–MA) [4, 7, 14].

Previously, the effects of functionalized PPs in the PP matrix (Scheme 1), such as PP–MA and hydroxy group-functionalized PP (PP–OH), on the interfacial shear strength of a single CF composite model were investigated using a microdroplet test [15, 16]. The addition of PP–OH to the matrix increased the interfacial shear strength to a level comparable to that of PP–MA. In addition, the interfacial shear strengths of the three types of PP–MA with different crystallinities and succinic anhydride group contents were compared. The results indicated that the interfacial shear strength did not depend on the succinic anhydride group content; that is, there were no significant differences in the chemical interaction potencies. Instead, the interfacial shear strength depended on the crystallinity of PP–MA.

For injection-molded SCFRPs, the matrix polymer molecular chains are oriented during the injection molding flow process. Hence, the polymer orientation may result in a different interfacial adhesion behavior relative to the interfacial shear strength results obtained by the microdroplet test [15, 16]. However, to the best of our knowledge, no information exists regarding the impact of matrix polymer orientation induced by shear flow in injection molding on the interfacial adhesion properties.

In this study, we investigated the effects of adding different types of functionalized PP specimens to the matrix on the tensile strength of injection-molded SCFRPs. A comparative analysis was performed on the factors related to the tensile strength of SCFRP, such as fiber length, fiber dispersity, fiber orientation, and crystallinity (mechanical properties of the PP matrix). In addition, the interfacial adhesion between the SCF and matrix of the PP resin was evaluated by the fracture surfaces of the SCFRPs after the tensile test. A relationship between the functionalized PP and interfacial adhesion of the SCFRPs was discussed in terms of the molecular orientation of the PP matrix.

Table 1 Properties of functionalized PPs and iPP

Samples	M_w	Acid value (mg KOH/g)	$X_{c,DSC}$[a]	T_m (°C)[a]
PP-t-OH	4×10^4	–	0.55	159
PP-t-MA	4×10^4	5	0.52	159
PP-g-MA1	3×10^4	52	0.37	140
PP-g-MA2	3.6×10^4	41	0.50	165
iPP	2.1×10^5	–	0.48	164

[a]Measured by DSC on the second heating scan

Experimental procedures

Materials

Functionalized PPs (hydroxy terminated telechelic PP (PP-t-OH) and succinic anhydride-terminated telechelic PP (PP-t-MA)) were obtained from San-ei Kogyo Co. (Saitama, Japan). Similarly, two conventional maleic anhydride-grafted PPs (PP-g-MA1; UMEX 1010 and PP-g-MA2; RIKEAID MG-400P) were obtained from Sanyo Chemical Industries, Ltd (Kyoto, Japan) and Riken Vitamin Co., Ltd (Tokyo, Japan). Isotactic PP (iPP; Z101S) with a melt flow rate of 25 g/10 min was supplied by Sumitomo Chemical Co. Ltd (Tokyo, Japan). The parameters of the functionalized PPs and iPP are listed in Table 1.

SCF (TR066A B4E) was supplied by Mitsubishi Chemical Co. (Tokyo, Japan) and used as received. The tensile modulus, tensile strength, fiber length, density and filament diameter of SCF were 224 GPa, 3730 MPa, 6 mm, 1.81 g/cm^3, and 7 μm, respectively.

Commercial iPP was blended with each functionalized PP (PP-t-OH, PP-t-MA, PP-g-MA1, and PP-g-MA2) and SCF using a corotating twin-screw extruder (ULT nano, Technovel Co., Osaka, Japan) to form a continuous strand. This strand was then water-cooled and pelletized to obtain PP matrices and SCFRP, that is, PP/SCF composites. The screw diameter and length-to-diameter ratio were 15 mm and 15, respectively. The barrel temperature and screw rotation speed were 200 °C and 200 rpm, respectively. The weight ratio of functionalized PP to iPP was 10:90 (wt.%). The SCF content was 10 vol% of the total composite composition. The mixed specimens of iPP, PP-t-OH, and SCF were abbreviated as iPP/PP-t-OH/SCF, with the others being similarly defined. Pelletized formulations were injection-molded using an injection molding machine (NP7 RealMini; Nissei Plastic Industrial Co., Ltd., Nagano, Japan), with dumbbell-shaped specimens being prepared for tensile testing. The conditions and shapes of the dumbbell-shaped specimens are provided in paragraph *S1* of the Supplementary Material.

Characterization

The volume fraction of the fiber (V_f) was measured according to JIS K 7075 using the burning method. The densities of PP/SCF specimens (ρ_c) were obtained via a hydrostatic weighting method using a density determination kit on a Mettler Toledo balance with hexane as an auxiliary liquid. The PP/SCF composite specimens (0.2–0.3 g) were burned at 350 °C for 4 h in an electric furnace to decompose the matrix PP resin, and the SCFs were recovered. V_f was calculated using the following equations (Eqs. 1–2):

$$W_f = \frac{w_2}{w_1} \times 100 \quad (1)$$

$$V_f = \frac{W_f \times \rho_c}{\rho_f} \quad (2)$$

where W_f, w_1, w_2, ρ_c, and ρ_f represent the weight fraction of the fiber, the weight of the PP/SCF specimen before decomposition, the weight of the recovered SCF strands, the density of the PP/SCF specimen, and the density of the SCF (1.81 g/cm^3), respectively.

The values of V_f of iPP/PP-t-OH/SCF, iPP/PP-t-MA/SCF, iPP/PP-g-MA1/SCF, iPP/PP-g-MA2/SCF and iPP/SCF were 9.4%, 9.8%, 9.6%, 10.2%, and 9.4%, respectively, and all PP/SCF specimens exhibited values of approximately $V_f = 10\%$, as expected.

Tensile tests of the dumbbell-shaped specimens were conducted using a universal testing machine (Autograph AGS-J; Shimadzu Co., Kyoto, Japan) at a crosshead speed of 5 mm/min. At least five specimens were tested per type. After tensile testing, the fracture surface was observed using a scanning electron microscope (SEM; S-3400N, Hitachi, Tokyo, Japan) at an accelerating voltage of 10.0 kV after gold sputtering.

The fiber orientations of the PP/SCF dumbbell-shaped specimens were measured as follows. The PP/SCF specimens were embedded in unsaturated polyester resins and subsequently polished using a rotary surface grinding machine. In addition, the length distributions of the fibers in the PP/SCF dumbbell-shaped specimens were quantified with the recovered SCFs using the above burning method for measuring V_f. The recovered SCFs were dispersed in ethanol and coated on a glass slide to quantify the lengths of the fibers. Images of the cross sections of the PP/SCF composites and dispersed fibers were captured using a microscope (VHX-2000, Keyence, Osaka, Japan). The orientations of the fibers were analyzed using ImageJ software from the microscopy images of cross section, and the over 450 samples were evaluated. The lengths of the fibers were analyzed using software (VHX-2000 analysis software; Keyence, Osaka, Japan), and a total of 600 samples were evaluated.

Differential scanning calorimetry (DSC) was performed with a Thermo Plus DSC 8230 L (Rigaku, Tokyo, Japan) to determine the crystallinity (X_c) values of the PP resins and PP/SCF composites. The temperature ranged from −20 °C to +220 °C, and the heating/cooling rate was 10 °C/min in a nitrogen atmosphere. The crystallinity was determined using Equation 3:

$$X_c = \frac{\triangle H}{\triangle H_{total} \times (1 - W_f \times 0.01)} \quad (3)$$

where ΔH and ΔH_{total} represent the melting enthalpy calculated from the endothermic area, and the melting enthalpy of PP with a crystallinity of 100% (209 J/g) [17], respectively.

The PP matrix orientations in the PP/SCF composites were determined and the polarized Raman scattering measurements were conducted using micro-Raman spectroscopy (LabRAM HR-800, HORIBA Jobin Yvon Ltd., Kyoto, Japan) with a He–Ne laser beam operating at 632.8 nm. The power of the laser beam was approximately 1.7 mW, with a focal length of 800 mm. The confocal hole size was 200 µm, and the spectrometer slit was set to 100 µm. A grating with 600 lines mm^{-1} and a 10× objective was used. For the measurements, PP/SCF specimens were embedded in polyester resin and subsequently polished using a rotary surface grinding machine. Polarized Raman analysis conditions and measurement areas are described in paragraph *S2* of the Supplementary Materials.

X-ray photoelectron spectroscopic (XPS) analysis was carried out in a JPS-9010 (JEOL, Ltd, Tokyo, Japan) to characterize the surface chemistry of SCF. The X-ray source was Mg Kα (10 kV, 100 W). The pass energies for the survey and narrow scan were 50 eV and 30 eV, respectively. To quantify the chemical composition of the SCF surface, the C1s spectrum was obtained in the narrow scan and deconvoluted using a Gaussian–Lorentz function after Shirley background removal.

Results and discussion

Tensile properties

The tensile stress–strain curves of PP resins without CF are shown in Fig. 1a. All PP specimens demonstrated ductile behavior and broke at approximately 580–700%. As shown in Fig. 1b, the average tensile yield stress of all PP matrices was ~30 MPa, regardless of the type of the added functionalized PPs, with no significant differences observed.

The tensile stress–strain curves of the PP/SCF composites are shown in Fig. 2a. Compared with the tensile

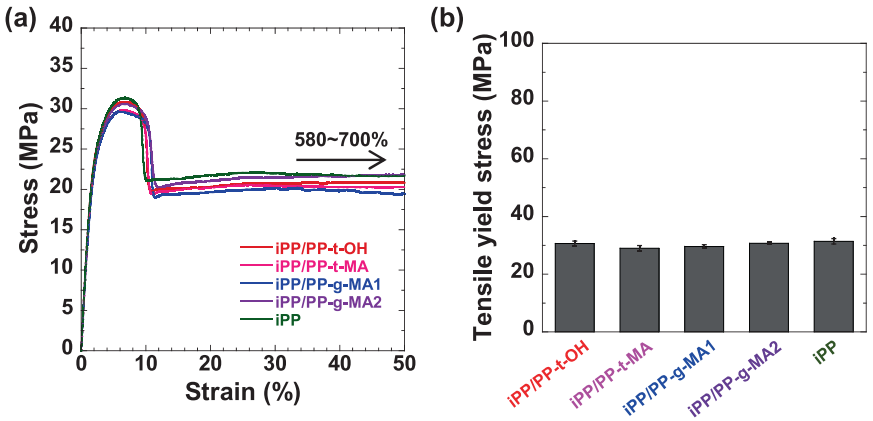

Fig. 1 Results of tensile tests of PP resins: **a** stress–strain curves and **b** average tensile yield stress

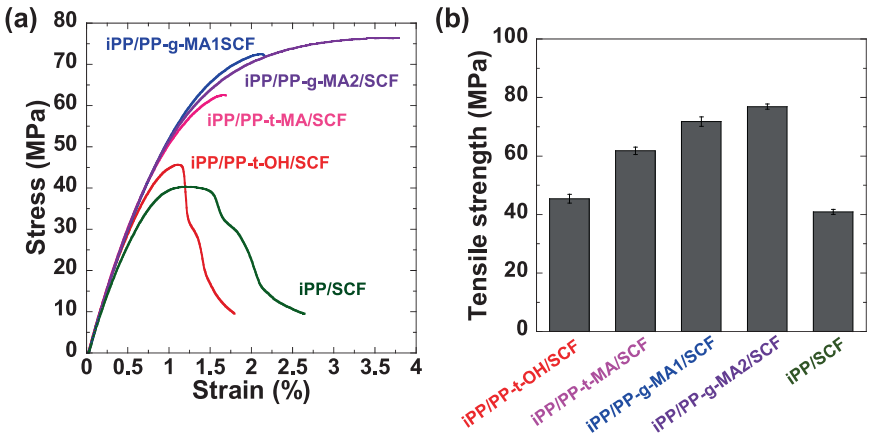

Fig. 2 Results of tensile tests of PP/SCF composites: **a** stress–strain curves and **b** average tensile strength

behaviors of PP resins, all PP/SCF composites exhibited brittle behaviors and significant decreases in stress at relatively low strains. Figure 2b indicates that the tensile strengths of all PP/SCF composites were higher than the tensile yield stress of PP because of the reinforcing effect of the SCF. However, significant differences in the tensile strength of PP/SCF composites were shown depending on the type of functionalized PPs added to the matrix despite the tensile yield stresses of all PP resin specimens without SCFs being approximately the same. iPP/SCF without functionalized PP displayed the lowest tensile strength, whereas iPP/PP-g-MA2/SCF exhibited the highest tensile strength. The addition of functionalized PPs improved the tensile strength of PP/SCF, and the extent of this increase depended on the type of functionalized PP added.

Orientation, dispersity, and length of fibers

The orientation, dispersity and length parameters of fibers are closely related to the tensile strength of PP/SCF [1–3, 5, 6, 8–11, 18, 19]. First, the fiber orientations were measured using microscopy images of the cross sections of the PP/SCF dumbbell specimens. The fibers were more oriented along the flow direction near the surface than in the central region in all PP/SCF composites, and there seemed to be no significant differences among specimens based on the appearance of the cross-sectional images (Fig. 3). From the results of the comparisons of the cumulative fiber orientation distributions (Fig. S3) and orientation parameters (Table S1), as specified in paragraph *S3* of the Supplementary Materials, fiber orientation did not depend on the tensile strength.

From the cross-sectional images of Fig. 3, the fiber lengths were considerably shorter than the original fiber length (6 mm) because they were damaged by the strong shear stress of the rotation process for all PP/SCF composites. However, all SCFs were separated into single-filament conditions with good dispersity, and identical dispersity among all PP/SCF composites was observed.

The cumulative SCF length distributions and the average fiber length are shown in Fig. S4 and Table S2, respectively, in paragraph *S4* of the Supplementary Material. The longer fiber length led to better strength of the PP/SCF composites. However, no correlation was found between the fiber length and tensile strength of the PP/SCF composites. Therefore, the differences in the influences of the type of functionalized PPs on the tensile strength with respect to fiber orientation, fiber dispersity and fiber length were small.

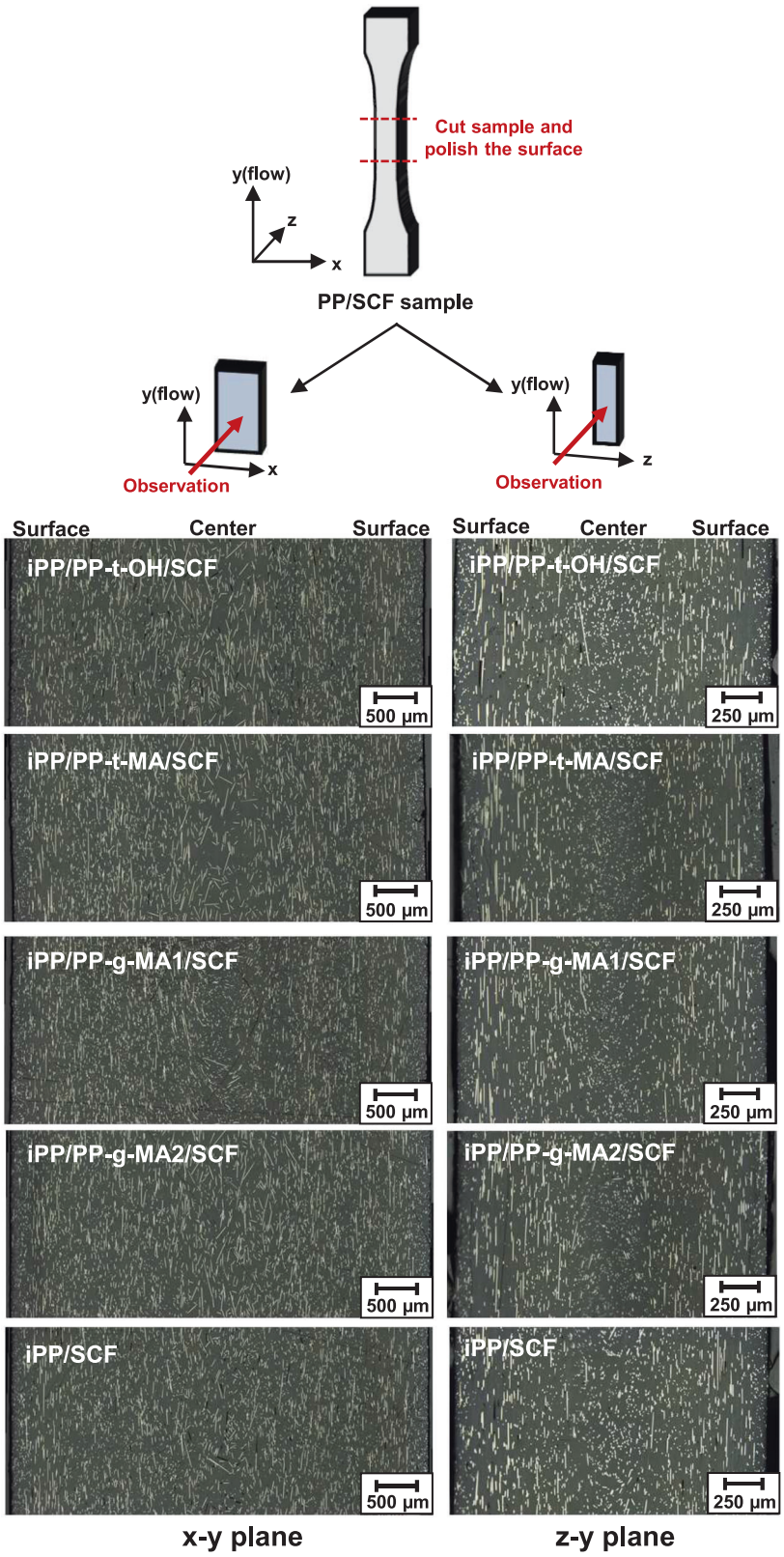

Fig. 3 Cross-sectional microscopy images of PP/SCF composites in the *x*–*y* and *z*–*y* planes

Table 2 Parameters of melting temperature (T_m), melting enthalpy (ΔH_m) and crystallinity (X_c)

Samples	T_m (°C)	ΔH_m (J/g)	X_c (-)
iPP/PP-t-OH/SCF	167.1	74.08	0.43
iPP/PP-t-MA/SCF	166.1	77.09	0.45
iPP/PP-g-MA1/SCF	167.3	71.39	0.41
iPP/PP-g-MA2/SCF	166.7	78.51	0.46
iPP/SCF	166.6	75.08	0.43
iPP/PP-t-OH	166.7	94.95	0.45
iPP/PP-t-MA	166.9	90.96	0.44
iPP/PP-g-MA1	168.3	86.72	0.42
iPP/PP-g-MA2	166.2	93.17	0.45
iPP	167.9	95.10	0.46

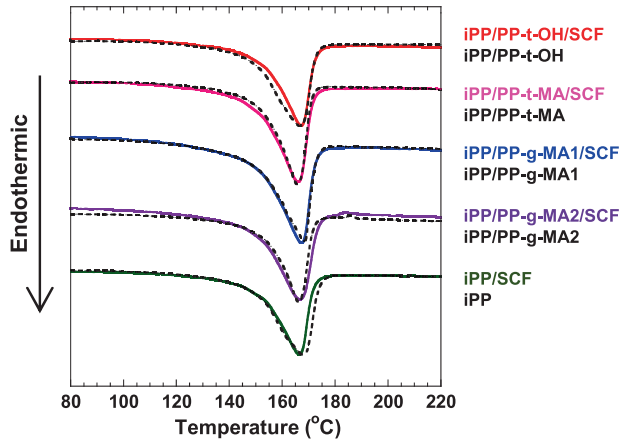

Fig. 4 DSC thermograms of PP/SCF composites and PP resins

Crystallinity of PP matrices in PP/SCF composites

For crystalline polymers such as PPs, the X_c values of matrices affect the mechanical properties, including the tensile strength. In general, a higher X_c leads to a higher tensile strength. In PP/SCF composites, the presence of SCF may affect the X_c of the PP matrix; therefore, the X_c of PP and PP/SCF were evaluated. In this study, injection-molded dumbbell specimens were cut into small pieces using a knife and analyzed using DSC. The melting parameters measured in the first heating scan are listed in Table 2, and the DSC thermograms of the PP resins and PP/SCF composites are shown in Fig. 4.

Table 2 indicates that the difference X_c of the neat PP resins between the highest iPP and lowest iPP/PP-g-MA1 was approximately 0.04; the effect of this difference in crystallinity on the tensile yield stress was almost negligible, as shown in Fig. 1. The X_c values of PP/SCF composites had to be different from the corresponding X_c values of PP resins if they significantly influenced the differences in tensile properties. However, the difference in X_c between each PP resin and its corresponding PP/SCF was small, with a value of less than 0.03.

Incidentally, the crystal size distribution affected the shape of the melting peak [20]. As shown in Fig. 4, the melting behaviors of all PP/SCF composites were similar to those of the corresponding PP resins, although the melting peaks of iPP/PP-t-OH/SCF and iPP/SCF appeared to be slightly sharper when containing SCF. In addition, the melting temperature (T_m) was influenced by crystalline forms, such as the monoclinal α-phase and hexagonal β-phase [21]. There were no significant differences in T_m between the PP resins and the corresponding PP/SCF composites (Table 2); this finding indicated that the crystalline forms of the PP matrix in the PP/SCF composites were the same as those of the corresponding PP resins.

In previous studies, it was reported that SCF acted as a nucleating agent for the crystallization of the PP matrix, even in PP/SCF composites with a low content of SCF [22]. However, excess SCF content decreased crystallinity relative to the neat PP matrix since CF could act as a restriction site for PP chains, hindering the formation of ordered crystalline structures [4, 22]. However, this experimental result showed that changes in the mechanical properties of the PP matrices in the PP/SCF composites were negligible compared with the PP resins because the changes in the X_c were very small.

Interfacial adhesion of PP/SCF composites

The interfacial shear strength attributed to the interfacial adhesion is related to the tensile strength of PP/SCF. Fracture surfaces of PP/SCF composites after the tensile test were observed to compare their interfacial adhesion characteristics. Figure 5a shows the central regions of the fracture surface from the top view; most fibers were pulled out from the PP matrix. The pulled-out SCFs had smooth surfaces without any remaining PP matrices (interfacial failure) in iPP/SCF and iPP/PP-t-OH/SCF. Furthermore, the specimens had oval cavities with diameters larger than those of the SCFs. These fractures indicated that poor interfacial adhesion caused interfacial failure and debonding, and subsequently, the PP matrix underwent plastic deformation before the complete fracture of the PP/SCF composites [4], resulting in the lowest tensile strength among all PP/SCF composites. For iPP/PP-t-MA/SCF and iPP/PP-g-MA1/SCF, interfacial and partially cohesive failures with thin PP matrix layers adhered to the SCF surface were observed. Cohesive failures with thick PP matrices adhering to the SCF surfaces were observed in iPP/PP-g-MA2/SCF. The differences in the failure modes of each PP/SCF composite suggested that the tensile strength was significantly dependent on the extent of interfacial adhesion. Given the functional groups of functionalized PPs, succinic anhydride

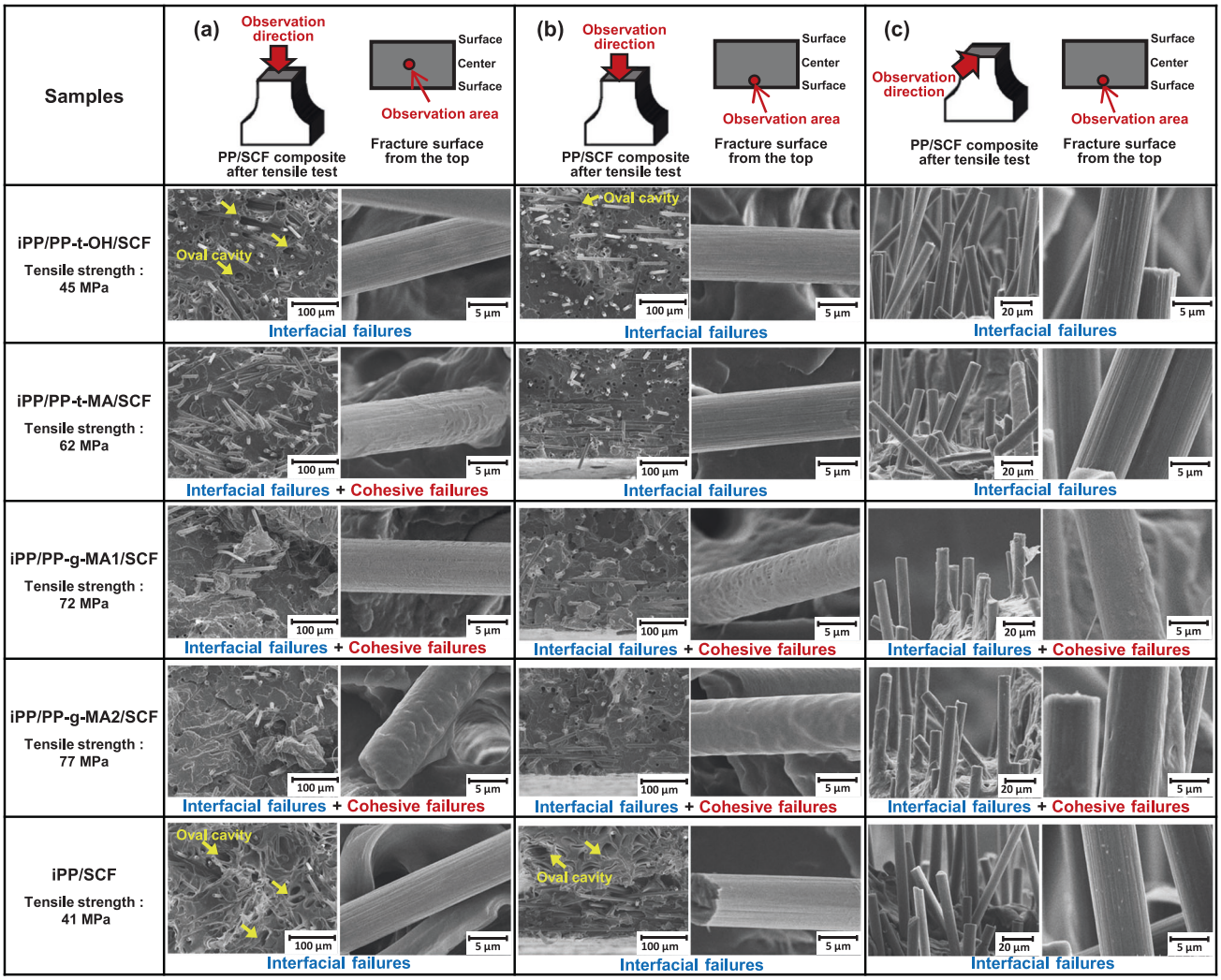

Fig. 5 SEM images of the fracture surfaces of PP/SCF composites: **a** in the central region from the top view, **b** near the surface from the top view, and **c** near the surface from the side view

groups were suggested to have higher interfacial adhesion than hydroxy groups, based on the failure mode and tensile strength of iPP/PP-t-MA/SCF and iPP/PP-t-OH/SCF. This phenomenon occurred because the succinic anhydride groups had better chemical interaction potency than the hydroxy groups. Only hydrogen bonds could be formed between hydroxy groups of PP-t-OH and CF surface functional groups, whereas both hydrogen and covalent bonds could be formed for PP-t-MA [15, 16]. iPP/PP-g-MA1/SCF and iPP/PP-g-MA2/SCF with higher functional group contents exhibited higher tensile strengths when PP-t-MA, PP-g-MA1, and PP-g-MA2 with functionalized PPs containing the same functional groups (succinic anhydride groups) were compared. The succinic anhydride group content could be related to the development of interfacial adhesion in injection-molded PP/SCF composites; however, failure occurrences in the central regions between iPP/PP-t-MA/SCF and iPP/PP-g-MA1/SCF did not show significant differences and relationships with tensile strength. Therefore, we compared the interfacial adhesion near the surface with that in the central regions.

Figures 5b, c illustrates the fracture surfaces of the PP/SCF composites after the tensile test near the surface from the top and side views, respectively. Interfacial failures were observed in the iPP/PP-t-OH/SCF, iPP/PP-t-MA/SCF, and iPP/SCF specimens. Moreover, oval cavities were found near the surfaces of iPP/PP-t-OH/SCF and iPP/SCF in Fig. 5b. In contrast, cohesive failures were partially observed in iPP/PP-g-MA1/SCF and iPP/PP-g-MA2/SCF. Compared with iPP/PP-t-MA/SCF and iPP/PP-g-MA1/SCF, there were almost no differences in failure modes in Fig. 5a. However, in Fig. 5b, c, differences were observed: iPP/PP-t-MA/SCF exhibited interfacial failures and iPP/PP-g-MA1/SCF exhibited cohesive failures in some areas. Therefore, interfacial adhesion differences existed near the surface regions between iPP/PP-t-MA/SCF and

iPP/PP-g-MA1/SCF. In this case, it was suggested that iPP/PP-g-MA1/SCF had higher interfacial adhesion than iPP/PP-t-MA/SCF. Furthermore, even in the same iPP/PP-g-MA1/SCF specimen, the amount of the PP matrix adhered to the SCF surface was different between near the surface and in the central region, and a thicker PP matrix adhering was observed near the surface.

Incidentally, the SCFs of all PP/SCF composites were more oriented along the flow direction near the surface than in the central region, as shown in Fig. 3. In addition to the oriented SCF behavior near the surface, the PP matrix could be oriented near the surface. In previous studies, the molecular orientation of PP induced by the shear flow of injection-molded PP resins was evaluated using polarized optical microphotography [23], wide-angle X-ray diffraction [24], and Raman spectroscopy [25, 26]. These studies showed that the molecular orientation of PP near the surface of injection-molded PP resins was higher than that in the central region, i.e., skin–core structures were observed. In other words, skin–core structures of the PP matrix appeared in the PP/SCF composites and had a relationship between the molecular orientation of the PP matrix and the interfacial adhesion with the SCF surface.

The molecular orientation of the PP matrix was studied using polarized Raman spectroscopy, and the band intensity ratio (I_{809}/I_{841}) was used as the orientation parameter. The ratio of Raman bands at 809 cm^{-1}, originating from the C-C skeletal symmetric stretching mode ν_s(C–C), and 841 cm^{-1}, originating from the CH_2 lateral alkyl rocking mode $r(CH_2)$, was used to estimate the molecular orientation [25, 26]. The orientation behaviors of iPP/PP-t-MA/SCF and iPP/PP-g-MA1/SCF were compared, with the Raman band intensity behaviors shown in Fig. 6. Both PP/SCF composites had no significant differences in the orientation behaviors; however, they showed increased orientation near the surface (~300 μm) and decreased orientation toward the central region. Therefore, the skin–core structures of the PP molecular chains were confirmed. The I_{809}/I_{841} of the iPP

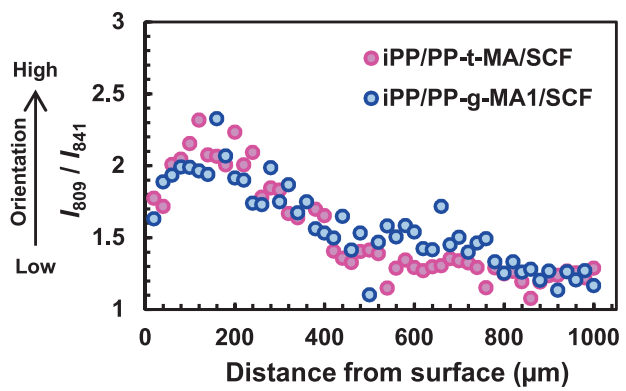

Fig. 6 Raman band intensity ratio (I_{809}/I_{842}) values of iPP/PP-t-MA/SCF and iPP/PP-g-MA1/SCF

film prepared by press molding without shear flow due to injection molding, i.e., nonorientation, was approximately 1.1. Hence, the PP molecular chains were oriented in the flow direction over a wide region of the PP/SCF composite.

Figure 5b, c shows that the interfacial adhesion of iPP/PP-g-MA1/SCF, which had partial cohesive failures, had a higher interfacial adhesion than iPP/PP-t-MA/SCF, which showed interfacial failures. One reason for this phenomenon could be the difference in the development of interfacial adhesion derived from chemical interactions, as shown in Fig. 7. The chemical structure of PP-t-MA was characterized by functional groups (succinic anhydride groups) attached at the end of the PP main chains, whereas PP-g-MA1 was characterized by the presence of some functional groups on the side chains. Chemical interactions reportedly included the formation of covalent (ester linkages) and hydrogen bonds between functional groups of the functionalized PP and hydroxy groups on the SCF surface [15]. The chemical conditions of the CF surface were analyzed by XPS, and the presence of hydroxy groups was exhibited (Fig. S5). In this case, it was suggested that PP-g-MA1, with more functional groups in the side chains, could have better chemical interactions, resulting in higher tensile strength. Near the surface of the PP/SCF composite in the highly oriented region, the difference in the degree of chemical interaction between iPP/PP-t-MA/SCF and iPP/PP-g-MA1/SCF was greater than that in the central region. This phenomenon could be attributed to the difference in fracture appearance. Incidentally, iPP/PP-g-MA2/SCF showed the highest tensile strength regardless of the slightly lower functional group content of PP-g-MA2 than that of PP-g-MA1. iPP/PP-g-MA2/SCF showed cohesive failures with thick PP adhering in the central region and near the surface of PP/SCF, i.e., the best interfacial properties. PP-g-MA2 was characterized by higher X_c and T_m values than PP-g-MA1 (Table 1). In a previous study, iPP/PP-g-MA2 exhibited higher local crystallinity at the interphase than iPP/PP-g-MA1, which improved the interfacial shear strength [15]. The local crystallinity at the interphase was sensitive to the nature of the functionalized PPs. The chemical interactions and the local crystallinity at the interphase could be associated with the highest tensile strength result of iPP/PP-g-MA2/SCF.

Differences in the results of the tensile strength derived from interfacial adhesion were significantly affected by the types and contents of functional groups of the functionalized PP added to the matrix. The interfacial shear strength of each PP matrix was measured using a single-filament composite specimen by the microdroplet method described in a previous study [15]. The interfacial shear strength was affected significantly by the crystallinity of the functionalized PP added to the matrix, not by that of the functional group contents. The PP matrices used in the microdroplet

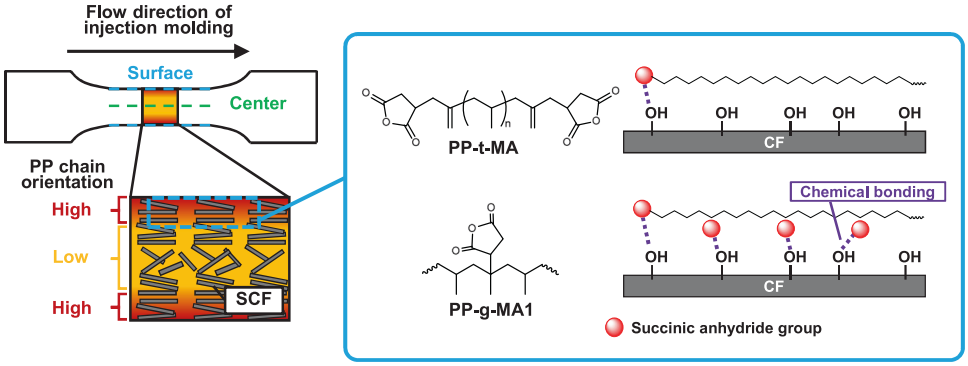

Fig. 7 Schematics of SCF and PP molecular orientation in PP/SCF composites and the inferred chemical bonding between the PP and CF surface functional groups near the surface

test were not exposed to shear flow as in the injection molding process, and the specimens were prepared by slow cooling. In other words, factors increasing interfacial adhesion differed between the single-filament composite specimen for microdroplet test and the injection-molded PP/SCF composites. Therefore, differences in the molding process of the composite specimens could change the development of the interfacial adhesion properties, even if the same type of functionalized PP was used as the matrix. These findings are useful for providing guidelines for designing suitable PP matrices and for developing high-performance CF-reinforced plastics under various molding conditions.

Conclusions

In this study, tensile tests were employed to compare injection-molded PP/SCF composites using four types of functionalized PPs. These functionalized PP variants featured distinct types and contents of functional groups (hydroxy groups or succinic anhydride) and crystallinities.

Our findings revealed that differences in the orientation, dispersity, and length of fibers and in the crystallinity of the PP matrix had negligible influences on the tensile strength disparities observed among the various types of functionalized PPs added to the matrix. Instead, the interfacial adhesion emerged as a critical determinant of tensile strength based on observations of the fracture surface after the PP/SCF tensile test. The types and contents of functional groups (hydroxy or succinic anhydride) introduced into the functionalized PP emerged as dominant factors influencing interfacial adhesion. In particular, functionalized PPs with many functional groups added to the side chains exhibited enhanced interfacial adhesion near the surface where the SCF and PP were highly oriented in parallel. These results highlighted the influences of PP molecular chain orientations, stemming from the shear flow during injection molding, on the interfacial adhesion of the PP matrix.

Acknowledgements The authors thank Riken Vitamin Co., Ltd (Tokyo, Japan) for supplying PP-g-MA2 and Dr. Daisuke Sasaki and Mr. Atsushi Takamura of San-ei Kogyo Co. (Saitama, Japan) for supplying PP-t-OH and PP-t-MA.

Funding Open access funding provided by University of Fukui.

Compliance with ethical standards

Conflict of interest The authors declare no competing interests.

Publisher's note Springer Nature remains neutral with regard to jurisdictional claims in published maps and institutional affiliations.

References

1. Rezaei F, Yunus R, Ibrahim NA. Effect of fiber length on thermomechanical properties of short carbon fiber reinforced polypropylene composites. Mater Des. 2009;30:260–3.
2. Fu SY, Lauke B, Ma¨der E, Yue CY, Hu X. Tensile properties of short-glass-fiber- and short-carbon-fiber-reinforced. Compos Part A Appl Sci Manuf. 2000;31:1117–25.
3. Fu SY, Lauke B, Ma¨der E, Yue CY, Hu X, Mai YW. Hybrid effects on tensile properties of hybrid short-glass-fiber-and short-carbon-fiber-reinforced polypropylene composites. J Mater Sci. 2001;36:1243–51.
4. Karsli NG, Aytac A. Effects of maleated polypropylene on the morphology, thermal and mechanical properties of short carbon fiber reinforced polypropylene composites. Mater Des. 2011;32:4069–73.
5. Hirano N, Muramatsu H, Inoue T. Research of fiber length and fiber-matrix adhesion in carbon fiber reinforced polypropylenes. J Jpn Soc Compos Mater. 2013;39:113–9.

6. Liu Y, Zhang X, Song C, Zhang Y, Fang Y, Yang B, et al. An effective surface modification of carbon fiber for improving the interfacial adhesion of polypropylene composites. Mater Des. 2015;88:810–9.
7. Wong KH, Mohammed DS, Pickering SJ, Brooks R. Effect of coupling agents on reinforcing potential of recycled carbon fibre for polypropylene composite. Compos Sci Technol. 2012;72:835–44.
8. Fukuda H, Chou TW. A probabilistic theory of the strength of short-fibre composites with variable fibre length and orientation. J Mater Sci. 1982;17:1003–11.
9. Fu SY, Lauke B. Effect of fiber length and orientation distribution on the tensile strength of short-fiber-reinforced polymers. Compos Sci Technol. 1996;56:1179–90.
10. Honma M, Tsuchiya A, Hirano N, Hashimoto T. Novel carbon-fiber-reinforced stampable thermoplastic sheet with high strength. Proceedings of the 18th International Conference on Composite Materials. Jeju, Korea, 2011:21–6.
11. Inoue A, Tanaka T, Arao Y, Taguchi H, Sawada Y. Optimization of screw design on fiber breakage and dispersion in injection molded bamboo-fiber-reinforced polypropylene. Kobunshi Ronbunshu. 2014;71:38–46.
12. Unterweger C, Duchoslav J, Stifter D, Fürst C. Characterization of carbon fiber surfaces and their impact on the mechanical properties of short carbon fiber reinforced polypropylene composites. Compos Sci Technol. 2015;108:41–7.
13. Seo HY, Cho KY, Im D, Kwon YJ, Shon M, Baek KY, et al. High mechanical properties of covalently functionalized carbon fiber and polypropylene composites by enhanced interfacial adhesion derived from rationally designed polymer compatibilizers. Compos Part B Eng. 2022;228:109439.
14. Kim JS, Kim DH. Compatibilizing effects of maleic anhydride-grafted-polypropylene (PP) on long carbon fiber-reinforced PP composites. J Thermoplast Compos Mater. 2015;28:1599–611.
15. Yamaguchi A, Urushisaki M, Uematsu H, Sakaguchi T, Hashimoto T. Effects of different types of maleic anhydride-modified polypropylene on the interfacial shear strengths of carbon fiber-reinforced polypropylene composites. Polym J. 2023;55:153–61.
16. Yamaguchi A, Hashimoto T, Uematsu H, Urushisaki M, Sakaguchi T, Takamura A, et al. Investigation of interfacial adhesion of telechelic polypropylenes for carbon fiber-reinforced plastics. Polym J. 2020;52:413–9.
17. Dudić D, Djoković V, Kostoski D. The high temperature secondary crystallisation of aged isotactic polypropylene. Polym Test. 2004;23:621–7.
18. Sanomura Y, Hayakawa K, Mizuno M, Kawamura M. Effect of Process Conditions on Young's Modulus and Strength of Extrudate in Short-Fiber-Reinforced Polypropylene. Seikei–Kakou. 2006;18:293–9.
19. Pipes RB, Mccullough RL, Taggart DG. Behavior of discontinuous fiber composites: fiber orientation. Polym Compos. 1982;3:34–9.
20. Nandan B, Kandpal LD, Mathur GN. Crystallization and melting behavior of poly(ether ether ketone)/poly(aryl ether sulfone) blends. J Appl Polym Sci. 2003;90:2906–18.
21. Tordjeman P, Robert C, Marin G, Gerard P. The effect of α, β crystalline structure on the mechanical properties of polypropylene. Eur Phys J E. 2001;4:459–65.
22. Wang C, Ying S. Thermal, tensile and dynamic mechanical properties of short carbon fibre reinforced polypropylene composites. Polym Polym Compos. 2013;21:65–71.
23. Kobayashi Y, Kanai T. Effect of injection molding cycle time on surface properties of polypropylene. Seikei–Kakou. 2010;22:97–103.
24. Ikura Y, Ito S, Sasaki H. Crystal orientation analysis of injection-molded polypropylene by micro-beam wide angle X-ray diffraction. Furukawa Electr Rev. 2020;51:18–23.
25. Martin J, Margueron S, Fontana M, Cochez M, Bourson P. Study of the molecular orientation heterogeneity in polypropylene injection-molded parts by Raman spectroscopy. Polym Eng Sci. 2009;50:138–43.
26. Akashige E, Usami T. Measurement of molecular orientation in injection-molded polypropylene by micro-raman spectroscopy. Anal Sci. 1991;7:1655–6.